metals

MDPI

Article

Long-Term in Vitro Corrosion of Biodegradable WE43 Magnesium Alloy in DMEM

Julia Nachtsheim [1], Jaka Burja [2,3,*], Songyun Ma [1,*] and Bernd Markert [1]

[1] Institute of General Mechanics (IAM), RWTH Aachen University, 52074 Aachen, Germany
[2] Institute of Metals and Technology, 1000 Ljubljana, Slovenia
[3] Department of Materials and Metallurgy, Faculty of Natural Sciences and Engineering, University of Ljubljana, 1000 Ljubljana, Slovenia
* Correspondence: jaka.burja@imt.si (J.B.); ma@iam.rwth-aachen.de (S.M.)

Abstract: The biodegradable WE43 magnesium alloy is an attractive biomedical material for orthopaedic implants due to its relatively high strength and corrosion resistance. Understanding the long-term corrosion behaviour in the human body plays a crucial role in the biomedical development and application of WE43 alloy for orthopaedic implants. In this work, the corrosion of an extruded WE43 magnesium alloy was investigated in a physiological environment using Dulbecco's Modified Eagle Medium's (DMEM) over a period of up to 10 weeks. To assess the in vitro corrosion process, we analysed the corrosion pits of the specimens' cross sections and the composition of the corrosion layer by scanning electron microscopy. The experimental results indicated that the long-term corrosion process of WE43 magnesium alloy consists of three stages: (1) The rapid corrosion stage within the first 7 days, (2) the steady corrosion stage between 7 and 28 days, (3) the accelerated corrosion stage between 28 and 70 days. The microchemical analysis revealed a heterogeneous three-layer corrosion product with varying thicknesses of 10 to 130 µm on the surfaces of the samples for all corrosion times. It is composed of an inner layer of Mg-O, an intermediate layer of Mg-O-Ca-P, and an outer layer of Mg-O-Ca-P-C. The corrosion layers have many microcracks that allow limited contact between the liquid medium and the surface of the alloy. In addition, microgalvanic corrosion was observed to cause corrosion pits between the intermetallic rare earth element-rich phases and the Mg matrix.

Keywords: biodegradable magnesium alloy; in vitro corrosion behaviour; WE43; pitting corrosion; DMEM

Citation: Nachtsheim, J.; Burja, J.; Ma, S.; Markert, B. Long-Term in Vitro Corrosion of Biodegradable WE43 Magnesium Alloy in DMEM. *Metals* **2022**, *12*, 2062. https://doi.org/10.3390/met12122062

Academic Editor: Damien Fabrègue

Received: 7 November 2022
Accepted: 29 November 2022
Published: 30 November 2022

1. Introduction

Biodegradable magnesium alloys are attractive biomedical materials in the field of implantology due to their excellent biocompatibility, biosafety, mechanical properties, and ability to degrade in the human body [1–5]. With their mechanical properties similar to native bone, magnesium alloys significantly reduce stress shielding caused by the high stiffness of implants, which leads to unphysiological small stress states in the bone and subsequently to a loss of bone density. More importantly, magnesium implants can obviate the need for a second implant removal surgery, which reduces health economic costs and patient morbidity compared to conventional implants. Furthermore, recent studies have revealed a positive mechanical integration and bone mass promotion at the osseous-implant interface [6,7]. However, their fast corrosion in the human body limits their application for orthopaedic implants.

A biodegradable implant should be designed to provide sufficient mechanical support to the fractured bone. Rapid corrosion in a physiological environment leads to excessive loss of mechanical integrity of magnesium orthopaedic implants during the bone healing process [8,9]. The WE43 magnesium alloy contains rare earth elements and zirconium, and has excellent mechanical properties, corrosion resistance, and biocompatibility. In comparison with other magnesium alloys such as AZ91, WE43 alloy shows a better corrosion

resistance in NaCl solution [10], higher tensile strength and ductility [11]. In addition, it is observed that WE43 exhibits higher fatigue limit in air and in physiological solution under cyclic loadings [11]. From a biocompatibility perspective, it is free of aluminium, which has been linked to diseases like Alzheimer's [12,13]. Additionally, it has been found that rare earth elements can improve the stress corrosion crack resistance of magnesium alloys [14]. Therefore, WE43 alloy is considered as a suitable candidate for the next-generation biomaterials for medical applications [15]. The corrosion resistance of magnesium alloys is significantly affected by their microstructure. Ageing, namely, increasing the amount of intermetallic precipitates negatively affects the corrosion resistance of WE43 alloy [16]. In addition, different surface modification methods are developed to control the degradation rate and improve the corrosion resistance of the alloy [10,17–21]. To adequately design the biodegradable orthopaedic implant of WE43 alloy, a deep understanding of the long-term corrosion mechanisms of the alloy in human body fluids is of importance.

The in vitro corrosion resistance of biodegradable metals is strongly influenced by the composition of the corrosive media [22–25]. Numerous in vitro experiments of biodegradable magnesium alloys have used inorganic simulated body fluid (SBF) as a corrosion medium [24–28], which possesses comparable ionic concentrations to human blood plasma. The high content of chlorides that are also present in human blood plasma have a detrimental effect on the corrosion resistance of magnesium and lead to severe pitting corrosion, since the magnesium hydroxide can be chemically converted into water-soluble magnesium chloride. Ascencio et al. [22] found that the formation of the different layers in modified SBF strongly influences the corrosion process as the substrate is protected by a reduced access of the aqueous medium. Yamamoto et al. [24] showed significant inhibition effect of organic compounds on the corrosion process. Wagener and Virtanen [29] compared the corrosion of magnesium in SBF and DMEM. In the experiments, they observed significantly slower corrosion and thinner calcium-phosphate-rich protective layers on the substrate surface in the DMEM environment. These calcium-phosphate-rich layers can interact with proteins, and thus further increase the corrosion resistance of WE43 alloy in DMEM [30]. Jin et al. [31] found a protective surface layer on WE43 alloy, consisting of an outer neodymium oxide and an inner magnesium oxide layer that initially retarded the corrosion in a DMEM medium containing proteins. In spite of the significant progress in the experimental studies of the short-term (predominantly up to 7 days) corrosion behaviour of magnesium alloys, the long-term corrosion behaviour of WE43 alloy in organic corrosion media has not been analysed intensively. It might be attributed to the easy microbial contamination of the organic media, which are breeding ground for microorganisms in aseptic conditions.

The present study focuses on the long-term corrosion of extruded WE43 magnesium alloy in an electrolyte that has a composition similar to the human blood plasma and includes organic compounds. For this purpose, in vitro corrosion experiments were conducted in DMEM at 37 °C for a period of up to ten weeks. A closed experimental environment in an incubator was used to ensure aseptic conditions. The corrosion was evaluated using scanning electron microscopy (SEM) of sample's cross sections. Additionally, the corrosion product was characterised by SEM and energy dispersive X-ray spectroscopy (EDS) microchemical analysis. The experimental results showed a nonlinear variation of the corrosion rates at different immersion times of up to ten weeks. The analysis of the corrosion products revealed a three-layer corrosion product consisting of an inner layer of Mg-O, an intermediate layer of Mg-O-Ca-P, and an outer layer of Mg-O-Ca-P-C. The new insight into the long-term corrosion behaviour of the alloy can be beneficial for assessing the corrosion behaviour of orthopaedic implants of WE43 alloy.

2. Materials and Methods

In the corrosion tests, round test specimens made of an extruded WE43 alloy with a diameter of 4 mm were used, which were provided by the company Medical Magnesium GmbH (Aachen, Germany). The chemical composition is given in Table 1. The samples were wrapped with teflon tape at both ends and sealed with heat shrink tubing to prevent corrosion. Therefore, only a uniform central area of the samples was exposed to the corrosion environment.

Table 1. Chemical composition of WE43 alloy.

Y	Nd	Zr	Al	Mn	Fe	Mg
3.8%	2.6%	0.02%	<0.01%	0.0025%	0.0065%	Bal.

To simulate the physiological environment, we used the cell culture medium DMEM (L0101-500, Biowest, Nuaillé, France) composed of inorganic as well as organic compounds. The composition of the DMEM is given in Table 2 and the ionic compositions of DMEM and blood plasma are compared in Table 3. The volume of the corrosion medium was chosen to provide stable corrosion conditions as suggested by Kirkland et al. [32]. Due to the use of organic media containing high levels of sugars, sterility conditions of the experimental setup are required for avoiding contaminations. Contaminations such as bacterial growth would shift the pH and change the associated physiological conditions. Therefore, 500 mL of the DMEM medium was supplemented with 5 mL Penicillin-Streptomycin (ThermoFisher Scientific Inc., Waltham, MA, USA) and 20 mg sodium azide (VWR International LLC, Radnor, PA, USA) to reduce the risk of infection with microorganisms. The DMEM contains phenol red as a colour indicator for visual control of the physiological regime of pH value.

Prior to the corrosion tests, the specimens were sterilised overnight in 80% ethanol and allowed to dry completely. Then, the samples were fixed at both ends in a funnel and immersed horizontally in the corrosion medium. Throughout the experiment, the corrosion experiment setup was placed in an incubator at 37 °C and 7% CO_2. The samples were immersed for 7, 14, 21, 28, and 70 days. After the corrosion test, the samples were removed from the medium, washed with demineralized water, and then with 80% ethanol.

Table 2. Composition of DMEM Medium.

Formulation	mg/L	Formulation	mg/L
Glycine	30	Magnesium Sulfate Anhydrous	97.67
L-Arginine Monohydrochloride	84	Potassium chloride	400
L-Cystine Dihydrochloride	62.6	Sodium Bicarbonate	3700
L-Histidine Monohydrochloride Monohydrate	42	Sodium Chloride	6400
L-Isoleucine	105	Sodium Phosphate Monobasic Anhydrous	109
L-Leucine	105	Choline Chloride	4
L-Lysine Monohydrochloride	146	D-Ca Pantothenate	4
L-Methionine	30	Folic Acid	4
L-Phenylalanine	66	Myo-Inositol	7.2
L-Serine	42	Nicotinamide	4
L-Threonine	95	Pyridoxal Hydrochloride	4
L-Tryptophan	16	Riboflavin	0.4
L-Tyrosine Disodium Salt Dihydrate	103.79	Thiamine Hydrochloride	4
L-Valine	94	D-Glucose Anhydrous	4500
Calcium Chloride Dihydrate	4265	Phenol Red Solution Salt	15.9
Ferric Nitrate Nonahydrate	0.1		

Table 3. Ionic concentrations in mmol/L.

Ion	Na^+	K^+	Mg^{2+}	Ca^{2+}	Cl^-	HCO_3^-	HPO_4^{2-}	SO_4^{2-}
Blood Plasma	142	5	1.5	2.5	103	27	1	0.5
DMEM	154	5.4	0.8	1.8	119	44	1	0.8

The cross sections were cut perpendicular to the sample axis within the corroded part of the samples, mounted in epoxy resin, and metallographically prepared by grinding and polishing. A scanning electron microscope SEM, Zeiss CrossBeam 550 (Carl Zeiss AG, Oberkochen, Germany) with an Octane Elite EDAX EDS microanalyzer (AMETEK, Inc., Berwyn, IL, USA) for energy-dispersive X-ray spectroscopy (EDS) was used for the analysis. The images of the cross sections were then processed using GeoGebra (GeoGebra Classic 5.0.720.0-d, Linz, Austria). The average sample radius was calculated using the measure at a minimum of 19 points along the circumference of the samples. Furthermore, the minimum radius was measured at the deepest pit and the maximal radius at the least corroded site.

3. Results and Discussion

The microstructure of WE43 alloy consists of the hexagonal close-packed α-Mg matrix and intermetallic precipitates, as shown in Figure 1. The intermetallic precipitates can be seen on the BSE image as white plates, rods and small spheres. The SEM EDS analysis shows that the larger plates have higher concentrations of yttrium, while the smaller particles are richer in Nd. The precipitates are small, less than 0.1 µm in diameter, which makes the EDS analysis less accurate as the analysis volume is relatively large, but it can be used as an indicator. The small intermetallic precipitates in WE43 alloy are typically β_1 (Mg_3(Y,Nd)) which are up to 100 nm in size and β ($Mg_{14}YNd_{22}$) as shown by Milkereit et al. [33]. The addition of rare earth elements strengthens the material and improves creep and corrosion resistance [34,35].

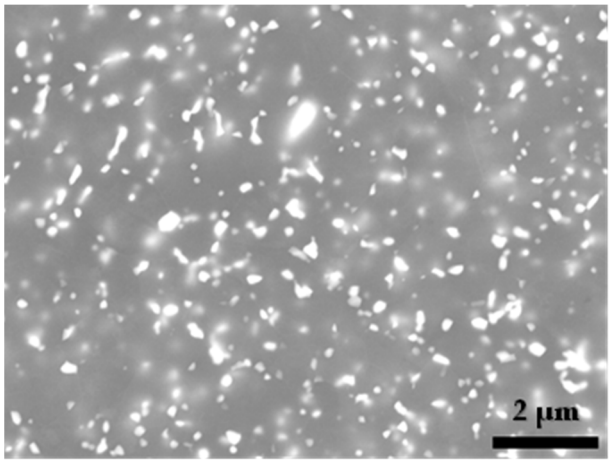

Figure 1. Microstructure of the uncorroded sample with the magnesium matrix and Y, Nd rich precipitates.

The images of the cross sections presented in Figure 2 show, that specimens have an initial smooth round shape. The diameter is 4 mm ± 1%. After the first week of corrosion, the corrosion surface is uneven indicating inhomogeneous corrosion, and corrosion pits appear along the circumference. The entire surface is covered by corrosion products of varying thickness. The corrosion surface of the cross sections of the samples that were corroded between 7 and 28 days hardly seem to change, which is also confirmed by the image analysis measurements. The analysis results of the measured diameters are shown in Figure 3. The radius of the least corroded site is shown with red dots, the diameter of the

most corroded site is shown in blue and the average radius with its standard deviation is shown in black.

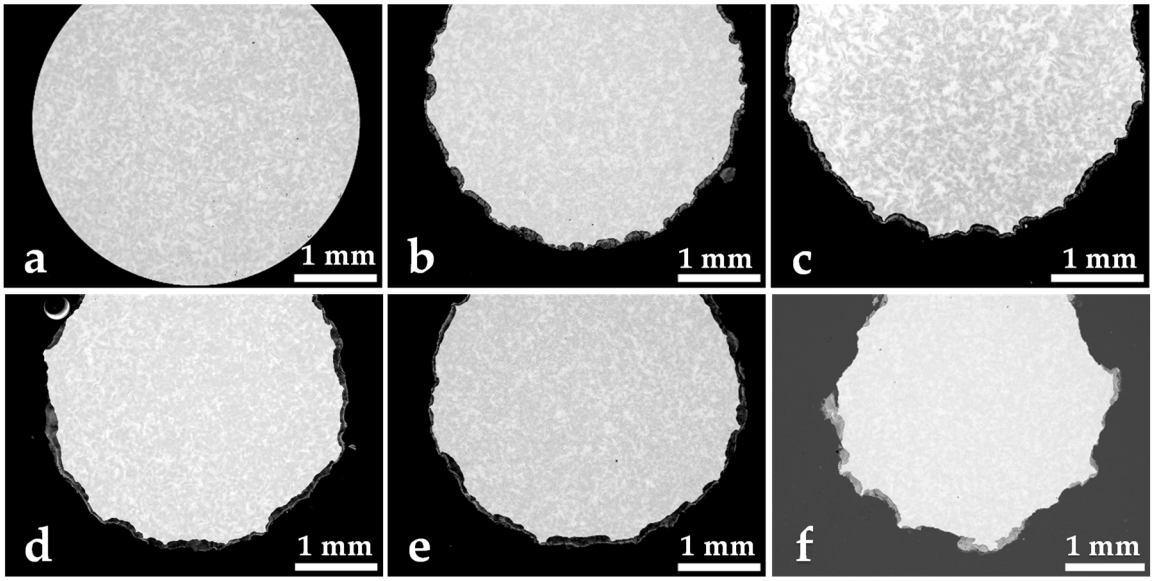

Figure 2. SEM BSE images of cross sections (perpendicular to the axis of the specimen) showing specimen before corrosion (**a**) and after 7 days (**b**), 14 days (**c**), 21 days (**d**), 28 days (**e**), or 70 days (**f**) of immersion time.

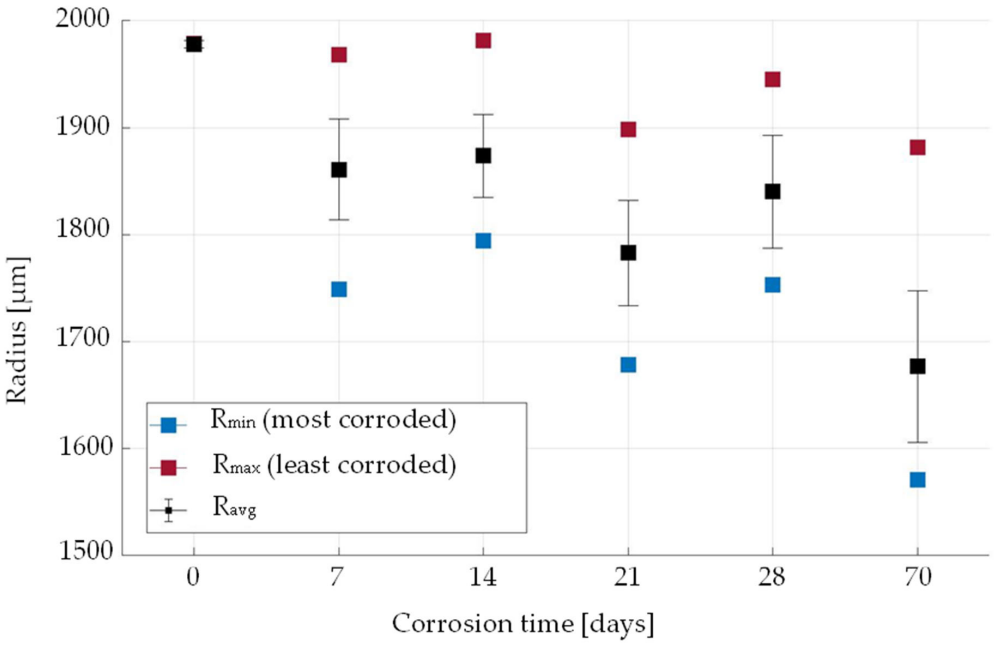

Figure 3. Image analysis of the cross sections. R_{min}: the radius at the most corroded spot in blue, R_{max}: the radius at the least corroded spot in red, and the average remaining radius R_{avg} of the specimen in black including the standard deviation.

After 7 days, the specimen's radius was reduced at its deepest pit by 11% and at its least corroded site by 6%, respectively. The cross-section analysis did not show any significant differences in pit depth between the 7-day and the 28-day corroded samples. In this corrosion stage, we observe noticeable reduction in the number of corrosion pits, which indicates a more homogeneous corrosion along the circumference. After 70 days they were significantly reduced by 21% and 15%, respectively, while the maximal radius

was not obviously affected compared to shorter corrosion times, since the intermetallic precipitates in the peaks resist corrosion.

The thickness of the corrosion product is not uniform on the surface, corrosion pits are covered by the corrosion layer with a thickness of 130 µm, while the least corroded areas have a corrosion layer with a thickness of less than 10 µm, as shown in Figure 4. The increased corrosion resistance of these peaks is attributed to microgalvanic corrosion due to the different potential of the Mg matrix and the intermetallic phases. The corrosion resistance of WE43 alloy in a physiological environment is much better than that of pure magnesium [34]. The rare earth elements in the WE43 alloy both enhance the corrosion resistance and slow down the corrosion process by stabilising the passive layer, especially presented in solid solution. However, galvanic coupling between the matrix and the intermetallic particles causes pitting corrosion [36]. Feng et al. [37] have clearly shown that the Mg matrix preferentially dissolves and acts as an anode in the microgalvanic corrosion couple with the second phase as a cathode, thus forming corrosion pits in NaCl solution. The formation of deep corrosion pits is difficult to detect on the sample surface and can only be observed in cut samples. Pitting corrosion significantly affects the mechanical integrity of the material and leads to premature failure. Localized pitting corrosion has no significant effect on the average corrosion rate, which relates to the entire sample surface and is difficult to detect with methods such as gas and mass loss measurements [31,38].

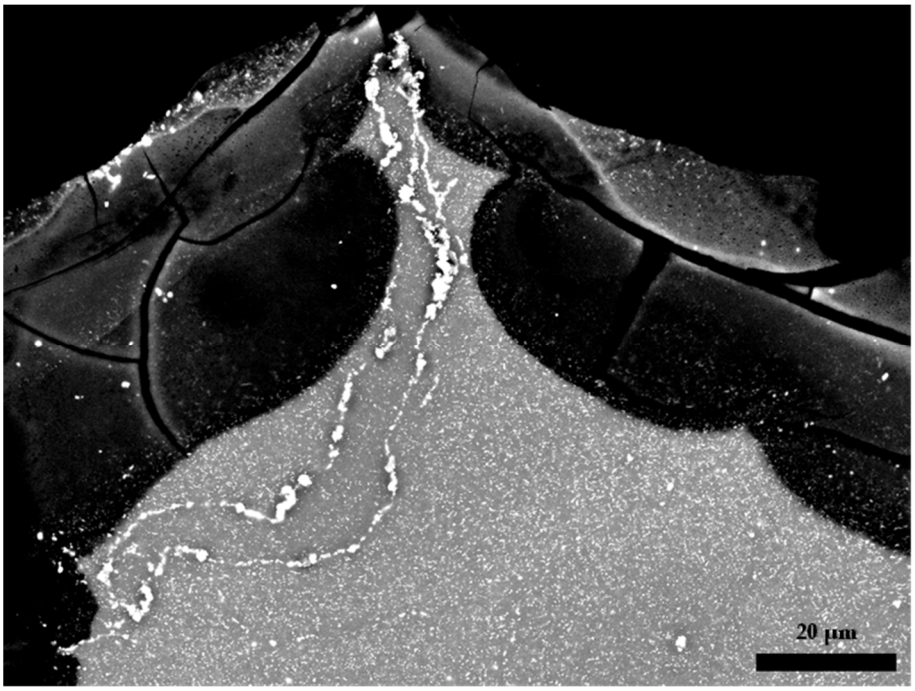

Figure 4. SEM BSE image of a sample corroded for 21 days, where microgalvanic corrosion is visible with the preferential dissolution of the α-Mg matrix, the white phases are Y and Nd rich intermetallic phases.

Figure 4 (after 21 days) clearly shows the preferential dissolution of the Mg matrix compared to the areas rich in intermetallic Mg-Y-Nd phases, which can be seen as white phases on the BSE SEM image. The areas richer in intermetallic phases are the products of chemical segregations in the alloy. Kalb et al. [39] analysed the corrosion of magnesium and WE43 alloy in simulated body fluid and discovered that H_2 gas forms at the intermetallic phase-rich cathode. They observed volcano-like structures after 3 min of corrosion and the remains of these structures were difficult to detect after 120 min. Since we have much longer corrosion times (7 days min), the structures could not be properly identified, but the cross-sectional ridges and peaks can be associated with them. It should also be emphasized that the distribution of the intermetallic phases is very uniform in the here used WE43 alloy.

In addition, the intermetallic precipitates are very fine compared to the material used in the study by Kalb [39]. This could be the reason for the less pronounced microgalvanic corrosion in our study. Nevertheless, microgalvanic corrosion occurs due to the presence of intermetallic phases, which act as cathode sites. Consequently, the dissolution of the Mg matrix can be described by the following anodic reactions. The anodic reactions are:

$$Mg + 2e^- \rightarrow Mg^{2+}, \quad (1)$$

$$2H_2O + 2e^- \rightarrow H_2 + 2OH^-, \quad (2)$$

$$Mg^{2+} + 2OH^- \rightarrow Mg(OH)_2. \quad (3)$$

The Mg^{2+} are mainly in the form of MgO. The equilibrium between the magnesium oxide and hydroxide can be described as:

$$MgO + 2OH^- \leftrightarrow Mg(OH)_2. \quad (4)$$

All corroded samples have the thickest corrosion product on the pits measuring about 130 µm. This stable thickness indicates that the corrosion product degrades over time. The analysis with higher magnifications in Figure 5 shows many microcracks in the corrosion layer leading to the detachment of the corrosion product. Furthermore, the cracks are linked to the alloy surface and can therefore be an important factor for the corrosion process. The observation of microcracks in the corrosion tests is consistent with the experimental study by Wagener and Virtanen [22]. The microcracks can be caused by the chemical reactions between the DMEM and the corrosion product, which increase the volume and cause stresses, or by the generation of hydrogen gas during magnesium hydroxide formation [39].

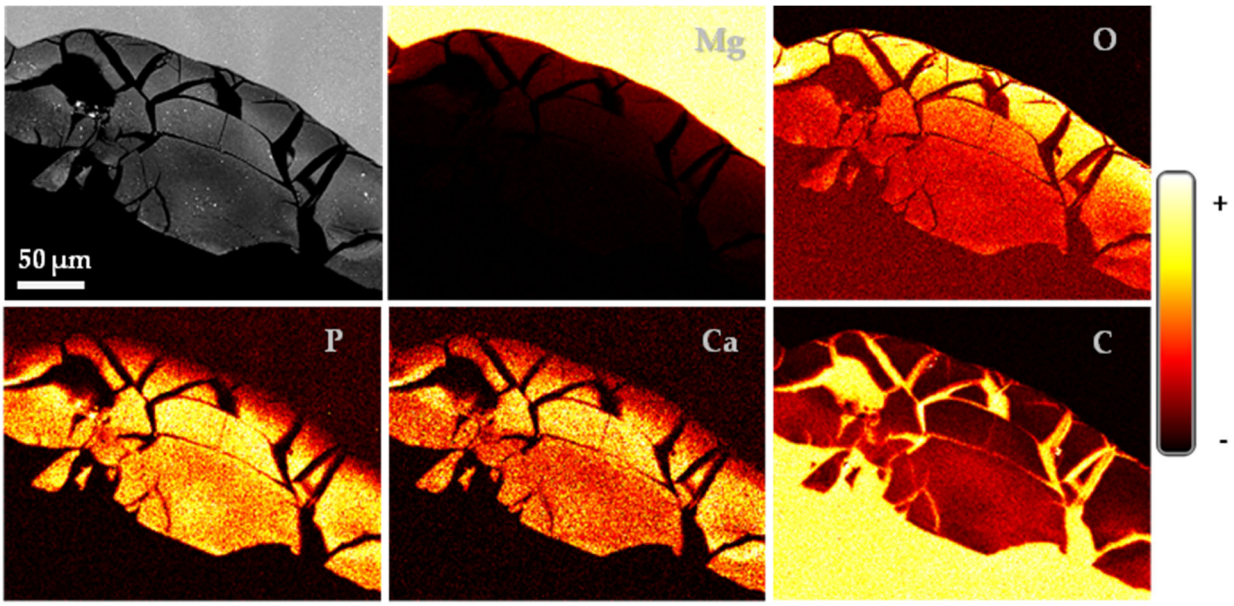

Figure 5. SEM EDS elemental mapping of cross sections of a 7-day corroded sample analysing the presence of Mg (top centre), O (top right), P (bottom left), Ca (bottom centre), and C (bottom right). High concentration levels are shown in yellow and low concentration levels in red.

The SEM EDS mapping shows that the corrosion product is heterogeneous. The differences in grey shading in the BSE image indicate differences in chemical composition. The differences are even clearer in the EDS mapping of Mg, O, P, Ca, and C. The limitations of EDS analysis must be considered as light elements such as H cannot be detected.

The SEM EDS elemental mapping (Figure 5) shows that the corrosion product consists of three different layers. As the matrix is rich in magnesium, which is very reactive, the

inner layer seems to be predominantly composed of Mg-O. The intermediate layer is enriched with Ca and P and the outer layer is additionally enriched with C. These three layers are observed in all corroded samples. The three layers indicate that the corrosion process starts with the formation of MgO, followed by penetration and chemical reaction of components of the medium with the oxidized layer. The reactions of the corrosion product with DMEM in turn result in the Ca- and P-enrichment. Finally, after sufficient exposure time, the outer layer is enriched with carbon. The carbon can be either in the form of carbonates or organic compounds such as glucose which are abundant in DMEM high glucose media. The corrosion progress appears to be controlled by the corrosion product cracking. The cracks are connected to the interface between the alloy and the corrosion product, which means that the supply of DMEM fluid is controlled by capillary forces. Such conditions limit the supply of oxygen and other components to the alloy surface, resulting in relatively slow corrosion progress. Figure 6 schematically shows the different layers of the corrosion product and the microcracks.

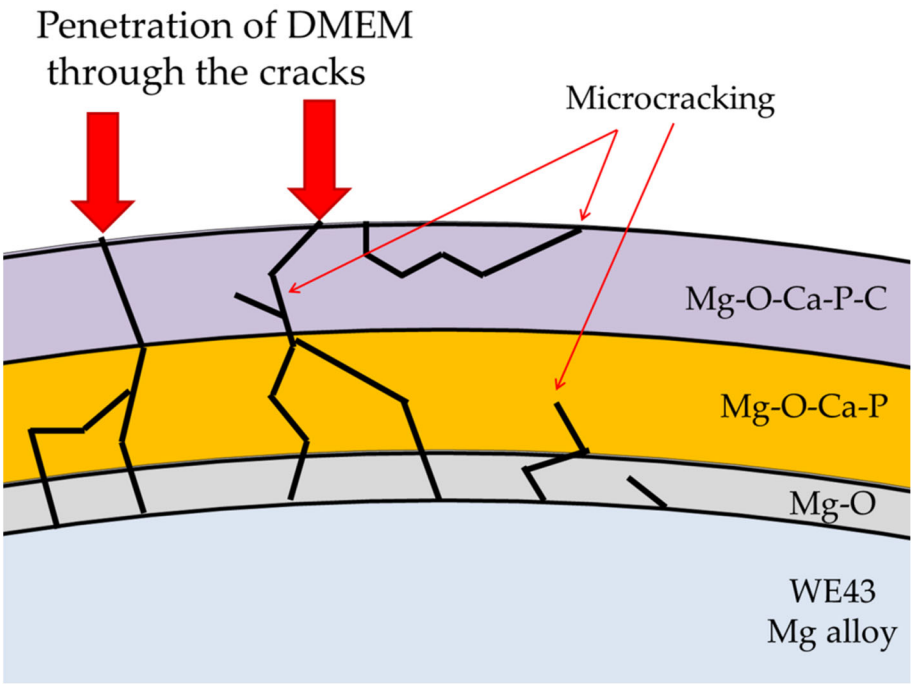

Figure 6. Schematic illustration of the three-layer corrosion product with microcracks in all corroded samples.

Ca is in the Ca^{2+} form, P is in the PO_4^{3-} form, while C is in the HCO_3^- form. Ca ions do not affect the corrosion of magnesium. However, calcium phosphates can form on the magnesium surface in DMEM, thus, inhibiting corrosion [11]. This finding is also interesting for biocompatibility, since calcium phosphate improves osseointegration [40]. The complexity of DMEM is clearly responsible for inhibiting the corrosion process compared to more simple inorganic solutions such as NaCl or SBF.

The phenol red in the DMEM is a sensitive colour indicator within the physiological regime and was used as an optical control of the pH during corrosion to ensure physiological conditions. The tests in this study were controlled at pH values between 7.3 and 7.7. In the case of magnesium hydroxide dissolution, the pH would increase. This would be a strong indicator of severe corrosion of the alloy. When the pH decreased, bacterial growth was observed and contaminated samples were excluded from this study. The stable pH values during the tests are consistent with the observed mild corrosion. The Pourbaix diagrams for magnesium state that at pH values above about 8.5 and up to 11.5 a protective oxide or hydroxide layer forms that slows the dissolution of Mg in aqueous

solutions [41]. This means that there is a local increase in pH at the first Mg-O layer that allows the formation of $Mg(OH)_2$, as observed by Kalb [39].

Furthermore, PO_4^{3+} and Ca^{2+}, nucleate and grow on the Mg surface at high pH levels. Phosphates with Mg/Ca attach themselves to the corrosion layer. The precipitation of the insoluble phosphates can be described as [42]:

$$H_nPO_4^{(3-n)+} + Mg^{2+} + Ca^{2+} + OH^- \rightarrow Mg_xCa_y\left(PO_4^{3+}\right)_z \quad (5)$$

The complicated Mg/Ca phosphates and MgO are here identified as the Mg-O-Ca-P layer.

4. Conclusions

In this study, long-term immersion tests over a period of up to 10 weeks were conducted in DMEM under physiological condition to investigate the in vitro corrosion behaviour of extruded WE43 magnesium alloy. Due to the use of organic media containing high levels of sugars, the in vitro experiments were vulnerable to contaminations and therefore carefully carried out under sterile conditions. The influence of contaminations such as bacterial growth was excluded in the experimental results.

To study the localized corrosion attack, we prepared SEM BSE images of specimens' cross-sections and evaluated the remaining radius along the samples' circumferences. We observed a nonlinear evolution of the corrosion damage in DMEM under physiological conditions. The long-term corrosion process of WE43 magnesium alloy consists of three stages: (1) the rapid corrosion within the first 7 days, (2) the steady corrosion between 7 and 28 days, and (3) the significantly accelerated corrosion between 28 and 70 days. The fast progress of the corrosion damage in the last stage is confirmed by the significant reduction of the sample radius of 21% at its deepest pit after 70 days. The present in vitro study on the corrosion behaviour of WE43 magnesium alloy reveals that the accelerated corrosion after long immersion times leads to severe corrosion damage. The initial rapid corrosion needs to be controlled for orthopaedic application, which can be achieved by applying surface coating on the alloy. After the stiffness and strength of the fractured bone recover to sufficient mechanical integrity, the accelerated corrosion in the final stage will mitigate the stress shielding effects during bone healing. The desired nonlinear variation of the corrosion enables an optimized design of the orthopedic implants for matching the bone healing process.

SEM EDS analysis of the corroded cross sections revealed a three-layer corrosion product consisting of an inner layer of Mg-O, an intermediate layer of Mg-O-Ca-P, and an outer layer of Mg-O-Ca-P-C. These layers were found consistently in all corroded samples for up to 10 weeks. The microcracks in the layers enable liquid medium penetration towards the alloy. The cracks also indicate mechanical instability of the corrosion product which appears to be about the same thickness inside the pits regardless of the corrosion times. Although the alloy exhibits a form of pitting corrosion driven by microgalvanic corrosion between the Mg matrix and the intermetallic phases, the resulting pits are shallow without severe localized corrosion.

Author Contributions: Conceptualization, J.N. and S.M.; methodology, J.N. and J.B.; validation, J.N., S.M., J.B. and B.M.; formal analysis J.N. and J.B.; investigation, J.N. and J.B.; resources, B.M.; data curation, J.N.; writing—original draft preparation, J.N. and J.B.; writing—review and editing, J.N., J.B., S.M. and B.M.; visualization, J.N.; supervision, S.M. and B.M.; project administration, J.N. and S.M.; funding acquisition, J.N., S.M. and B.M. All authors have read and agreed to the published version of the manuscript.

Funding: This research was funded by the Federal Ministry of Education and Research of Germany in the framework of RePlaSys (project number FKZ 13GW0352B).

Data Availability Statement: Not applicable.

Acknowledgments: The authors would like to thank Barbara Šetino Batič for support with SEM images and Thomas Derra for help with the corrosion experiments. We would like to thank Medical Magnesium GmbH for supplying the alloy.

Conflicts of Interest: The authors declare no conflict of interest. The funders had no role in the design of the study; in the collection, analyses, or interpretation of data; in the writing of the manuscript; or in the decision to publish the results.

References

1. Waksman, R.; Pakala, R.; Kuchulakanti, P.K.; Baffour, R.; Hellinga, D.; Seabron, R.; Tio, F.O.; Wittchow, E.; Hartwig, S.; Harder, C.; et al. Safety and Efficacy of Bioabsorbable Magnesium Alloy Stents in Porcine Coronary Arteries. *Catheter. Cardiovasc. Interv.* **2006**, *68*, 607–617. [CrossRef] [PubMed]
2. Erdmann, N.; Angrisani, N.; Reifenrath, J.; Lucas, A.; Thorey, F.; Bormann, D.; Meyer-Lindenberg, A. Biomechanical Testing and Degradation Analysis of MgCa0.8 Alloy Screws: A Comparative in Vivo Study in Rabbits. *Acta Biomater.* **2011**, *7*, 1421–1428. [CrossRef] [PubMed]
3. He, Y.; Tao, H.; Zhang, Y.; Jiang, Y.; Zhang, S.; Zhao, C.; Li, J.; Zhang, B.; Song, Y.; Zhang, X. Biocompatibility of Bio-Mg-Zn Alloy within Bone with Heart, Liver, Kidney and Spleen. *Chin. Sci. Bull.* **2009**, *54*, 484–491. [CrossRef]
4. Feyerabend, F.; Fischer, J.; Holtz, J.; Witte, F.; Willumeit, R.; Drücker, H.; Vogt, C.; Hort, N. Evaluation of Short-Term Effects of Rare Earth and Other Elements Used in Magnesium Alloys on Primary Cells and Cell Lines. *Acta Biomater.* **2010**, *6*, 1834–1842. [CrossRef] [PubMed]
5. Gu, X.; Zheng, Y.; Cheng, Y.; Zhong, S.; Xi, T. In Vitro Corrosion and Biocompatibility of Binary Magnesium Alloys. *Biomaterials* **2009**, *30*, 484–498. [CrossRef] [PubMed]
6. Witte, F.; Kaese, V.; Haferkamp, H.; Switzer, E.; Meyer-Lindenberg, A.; Wirth, C.J.; Windhagen, H. In Vivo Corrosion of Four Magnesium Alloys and the Associated Bone Response. *Biomaterials* **2005**, *26*, 3557–3563. [CrossRef]
7. Castellani, C.; Lindtner, R.A.; Hausbrandt, P.; Tschegg, E.; Stanzl-Tschegg, S.E.; Zanoni, G.; Beck, S.; Weinberg, A.M. Bone-Implant Interface Strength and Osseointegration: Biodegradable Magnesium Alloy versus Standard Titanium Control. *Acta Biomater.* **2011**, *7*, 432–440. [CrossRef]
8. Witte, F.; Eliezer, A. Biodegradable Metals. *Degrad. Implant Mater.* **2012**, *9781461439*, 93–109. [CrossRef]
9. Gu, X.N.; Zheng, Y.F. A Review on Magnesium Alloys as Biodegradable Materials. *Front. Mater. Sci. China* **2010**, *4*, 111–115. [CrossRef]
10. Arrabal, R.; Matykina, E.; Viejo, F.; Skeldon, P.; Thompson, G.E. Corrosion Resistance of WE43 and AZ91D Magnesium Alloys with Phosphate PEO Coatings. *Corros. Sci.* **2008**, *50*, 1744–1752. [CrossRef]
11. Gu, X.N.; Zhou, W.R.; Zheng, Y.F.; Cheng, Y.; Wei, S.C.; Zhong, S.P.; Xi, T.F.; Chen, L.J. Corrosion Fatigue Behaviors of Two Biomedical Mg Alloys—AZ91D and WE43—In Simulated Body Fluid. *Acta Biomater.* **2010**, *6*, 4605–4613. [CrossRef] [PubMed]
12. McDonald, J.B.; Dhakal, S.; Macreadie, I. A Toxic Synergy between Aluminium and Amyloid Beta in Yeast. *Int. J. Mol. Sci.* **2021**, *22*, 1835. [CrossRef] [PubMed]
13. Dey, M.; Singh, R.K. Neurotoxic Effects of Aluminium Exposure as a Potential Risk Factor for Alzheimer's Disease. *Pharmacol. Rep.* **2022**, *74*, 439–450. [CrossRef] [PubMed]
14. Kannan, M.B.; Dietzel, W.; Blawert, C.; Atrens, A.; Lyon, P. Stress Corrosion Cracking of Rare-Earth Containing Magnesium Alloys ZE41, QE22 and Elektron 21 (EV31A) Compared with AZ80. *Mater. Sci. Eng. A* **2008**, *480*, 529–539. [CrossRef]
15. Leleu, S.; Rives, B.; Bour, J.; Causse, N.; Pébère, N. On the stability of the oxides film formed on a magnesium alloy containing rare-earth elements. *Electrochim. Acta* **2018**, *290*, 586–594. [CrossRef]
16. Li, M.; Benn, F.; Derra, T.; Kröger, N.; Zinser, M.; Smeets, R.; Molina-Aldareguia, J.M.; Kopp, A.; LLorca, J. Microstructure, Mechanical Properties, Corrosion Resistance and Cytocompatibility of WE43 Mg Alloy Scaffolds Fabricated by Laser Powder Bed Fusion for Biomedical Applications. *Mater. Sci. Eng. C* **2021**, *119*, 111623. [CrossRef]
17. Imwinkelried, T.; Beck, S.; Iizuka, T.; Schaller, B. Effect of a Plasmaelectrolytic Coating on the Strength Retention of In Vivo and In Vitro Degraded Magnesium Implants. *Acta Biomater.* **2013**, *9*, 8643–8649. [CrossRef]
18. Zhao, Y.; Wu, G.; Lu, Q.; Wu, J.; Xu, R.; Yeung, K.W.K.; Chu, P.K. Improved Surface Corrosion Resistance of WE43 Magnesium Alloy by Dual Titanium and Oxygen Ion Implantation. *Thin Solid Films* **2013**, *529*, 407–411. [CrossRef]
19. Guo, L.F.; Yue, T.M.; Man, H.C. Excimer Laser Surface Treatment of Magnesium Alloy WE43 for Corrosion Resistance Improvement. *J. Mater. Sci.* **2005**, *40*, 3531–3533. [CrossRef]
20. Ye, C.H.; Zheng, Y.F.; Wang, S.Q.; Xi, T.F.; Li, Y.D. In Vitro Corrosion and Biocompatibility Study of Phytic Acid Modified WE43 Magnesium Alloy. *Appl. Surf. Sci.* **2012**, *258*, 3420–3427. [CrossRef]
21. Li, M.; Cheng, Y.; Zheng, Y.F.; Zhang, X.; Xi, T.F.; Wei, S.C. Surface Characteristics and Corrosion Behaviour of WE43 Magnesium Alloy Coated by SiC Film. *Appl. Surf. Sci.* **2012**, *258*, 3074–3081. [CrossRef]
22. Ascencio, M.; Pekguleryuz, M.; Omanovic, S. An Investigation of the Corrosion Mechanisms of WE43 Mg Alloy in a Modified Simulated Body Fluid Solution: The Influence of Immersion Time. *Corros. Sci.* **2014**, *87*, 489–503. [CrossRef]
23. Mueller, W.D.; Lorenzo De Mele, M.F.; Nascimento, M.L.; Zeddies, M. Degradation of Magnesium and Its Alloys: Dependence on the Composition of the Synthetic Biological Media. *J. Biomed. Mater. Res.—Part A* **2009**, *90*, 487–495. [CrossRef] [PubMed]

24. Yamamoto, A.; Hiromoto, S. Effect of Inorganic Salts, Amino Acids and Proteins on the Degradation of Pure Magnesium In Vitro. *Mater. Sci. Eng. C* **2009**, *29*, 1559–1568. [CrossRef]
25. Müller, L.; Müller, F.A. Preparation of SBF with Different HCO3- Content and Its Influence on the Composition of Biomimetic Apatites. *Acta Biomater.* **2006**, *2*, 181–189. [CrossRef] [PubMed]
26. Cao, G.; Zhang, D.; Zhang, W.; Zhang, W. In Vitro Corrosion Study of Friction Stir Processed WE43 Magnesium Alloy in a Simulated Body Fluid. *Materials* **2016**, *9*, 542. [CrossRef]
27. Ascencio, M.; Pekguleryuz, M.; Omanovic, S. An Investigation of the Corrosion Mechanisms of WE43Mg Alloy in a Modified Simulated Body Fluid Solution: The Effect of Electrolyte Renewal. *Corros. Sci.* **2015**, *91*, 297–310. [CrossRef]
28. Kannan, M.B.; Raman, R.K.S. In Vitro Degradation and Mechanical Integrity of Calcium-Containing Magnesium Alloys in Modified-Simulated Body Fluid. *Biomaterials* **2008**, *29*, 2306–2314. [CrossRef]
29. Wagener, V.; Virtanen, S. Influence of Electrolyte Composition (Simulated Body Fluid vs. Dulbecco's Modified Eagle's Medium), Temperature, and Solution Flow on the Biocorrosion Behavior of Commercially Pure Mg. *Corrosion* **2017**, *73*, 1413–1422. [CrossRef]
30. Höhlinger, M.; Christa, D.; Zimmermann, V.; Heise, S.; Boccaccini, A.R.; Virtanen, S. Influence of Proteins on the Corrosion Behavior of a Chitosan-Bioactive Glass Coated Magnesium Alloy. *Mater. Sci. Eng. C* **2019**, *100*, 706–714. [CrossRef]
31. Jin, W.; Wu, G.; Feng, H.; Wang, W.; Zhang, X.; Chu, P.K. Improvement of Corrosion Resistance and Biocompatibility of Rare-Earth WE43 Magnesium Alloy by Neodymium Self-Ion Implantation. *Corros. Sci.* **2015**, *94*, 142–155. [CrossRef]
32. Kirkland, N.T.; Birbilis, N.; Staiger, M.P. Assessing the Corrosion of Biodegradable Magnesium Implants: A Critical Review of Current Methodologies and Their Limitations. *Acta Biomater.* **2012**, *8*, 925–936. [CrossRef] [PubMed]
33. Milkereit, B.; Burgschat, L.; Kemsies, R.H.; Springer, A.; Schick, C.; Kessler, O. In Situ Differential Scanning Calorimetry Analysis of Dissolution and Precipitation Kinetics in Mg–Y–RE Alloy WE43. *J. Magnes. Alloy.* **2019**, *7*, 1–14. [CrossRef]
34. Pereira, G.S.; Koga, G.Y.; Avila, J.A.; Bittencourt, I.M.; Fernandez, F.; Miyazaki, M.H.; Botta, W.J.; Bose Filho, W.W. Corrosion Resistance of WE43 Mg Alloy in Sodium Chloride Solution. *Mater. Chem. Phys.* **2021**, *272*, 124930. [CrossRef]
35. Luo, K.; Zhang, L.; Wu, G.; Liu, W.; Ding, W. Effect of Y and Gd Content on the Microstructure and Mechanical Properties of Mg–Y–RE Alloys. *J. Magnes. Alloy.* **2019**, *7*, 345–354. [CrossRef]
36. Leleu, S.; Rives, B.; Causse, N.; Pébère, N. Corrosion Rate Determination of Rare-Earth Mg Alloys in a Na_2SO_4 Solution by Electrochemical Measurements and Inductive Coupled Plasma-Optical Emission Spectroscopy. *J. Magnes. Alloy.* **2019**, *7*, 47–57. [CrossRef]
37. Feng, B.; Liu, G.; Yang, P.; Huang, S.; Qi, D.; Chen, P.; Wang, C.; Du, J.; Zhang, S.; Liu, J. Different Role of Second Phase in the Micro-Galvanic Corrosion of WE43 Mg Alloy in NaCl and Na_2SO_4 Solution. *J. Magnes. Alloy.* **2021**, *10*, 1598–1608. [CrossRef]
38. Tsakiris, V.; Tardei, C.; Clicinschi, F.M. Biodegradable Mg Alloys for Orthopedic Implants—A Review. *J. Magnes. Alloy.* **2021**, *9*, 1884–1905. [CrossRef]
39. Kalb, H.; Rzany, A.; Hensel, B. Impact of Microgalvanic Corrosion on the Degradation Morphology of WE43 and Pure Magnesium under Exposure to Simulated Body Fluid. *Corros. Sci.* **2012**, *57*, 122–130. [CrossRef]
40. Schwarz, M.L.R.; Kowarsch, M.; Rose, S.; Becker, K.; Lenz, T.; Jani, L. Effect of Surface Roughness, Porosity, and a Resorbable Calcium Phosphate Coating on Osseointegration of Titanium in a Minipig Model. *J. Biomed. Mater. Res.—Part A* **2009**, *89*, 667–678. [CrossRef]
41. Pourbaix, M. *Atlas of Electrochemical Equilibria in Aqueous Solutions*, 2nd ed.; National Association of Corrosion Engineers: Houston, TX, USA, 1974.
42. Zhang, S.; Zhang, X.; Zhao, C.; Li, J.; Song, Y.; Xie, C.; Tao, H.; Zhang, Y.; He, Y.; Jiang, Y.; et al. Research on an Mg-Zn alloy as a degradable biomaterial. *Acta Biomater.* **2010**, *6*, 626–640. [CrossRef] [PubMed]